Available online at www.sciencedirect.com
SCIENCE DIRECT®
Journal of Solid State Chemistry 179 (2006) 217–225
JOURNAL OF SOLID STATE CHEMISTRY
www.elsevier.com/locate/jssc

Synthesis and properties of pyrazine-pillared $Ag_3Mo_2O_4F_7$ and $AgReO_4$ layered phases

Haisheng Lin, Bangbo Yan, Paul D. Boyle, Paul A. Maggard*

Department of Chemistry, North Carolina State University, Raleigh, NC 27695-8204, USA

Received 15 September 2005; received in revised form 18 October 2005; accepted 19 October 2005
Available online 28 November 2005

Abstract

The new pyrazine-pillared solids, $AgReO_4(C_4H_4N_2)$ (**I**) and $Ag_3Mo_2O_4F_7(C_4H_4N_2)_3$ ($C_4H_4N_2$ = pyrazine, pyz) (**II**), were synthesized by hydrothermal methods at 150 °C and characterized using single crystal X-ray diffraction (**I**—$P2_1/c$, No. 14, $Z = 4$, $a = 7.2238(6)$ Å, $b = 7.4940(7)$ Å, $c = 15.451(1)$ Å, $\beta = 92.296(4)^\circ$; **II**—$P2/n$, No. 13, $Z = 2$, $a = 7.6465(9)$ Å, $b = 7.1888(5)$ Å, $c = 19.142(2)$ Å, $\beta = 100.284(8)^\circ$), thermogravimetric analysis, UV-Vis diffuse reflectance, and photoluminescence measurements. Individual Ag(pyz) chains in **I** are bonded to three perrhenate ReO_4^- tetrahedra per layer, while each layer in **II** contains sets of three edge-shared Ag(pyz) chains (π–π stacked) that are edge-shared to four $Mo_2O_4F_7^{3-}$ dimers. A relatively small interlayer spacing results from the short length of the pyrazine pillars, and which can be removed at just slightly above their preparation temperature, at >150–175 °C, to produce crystalline $AgReO_4$ for **I**, and Ag_2MoO_4 and an unidentified product for **II**. Both pillared solids exhibit strong orange-yellow photoemission, at 575 nm for **I** and 560 nm for **II**, arising from electronic excitations across (charge transfer) band gaps of 2.91 and 2.76 eV in each, respectively. Their structures and properties are analyzed with respect to parent 'organic free' silver perrhenate and molybdate solids which manifest similar photoemissions, as well as to the calculated electronic band structures.

Keywords: Pillared; Layered; Perrhenate; Molybdate; Optical properties; Pyrazine; Extended Hückel calculations

1. Introduction

Synthetic routes to new solids with layered structures is often desired in order to probe the structural or physical property effects of intercalating or deintercalating guest molecules between the interlamellar regions. Envisioned or existing applications include rechargeable batteries, catalysts, separations, ion exchange, and gas absorption, to name a few—for reviews of the intercalation chemistry of layered solids, see [1]; for a few selected examples of recent research articles, see [2]. Pillared layered structures in the mixed metal-oxide/organic systems, for example, are constructed through the use of organic ligands that bridge (or pillar) across the metal sites within separated metal-oxide layers, predisposing the structure towards guest intercalation within the gallery or pillared areas. Chemical systems which feature layered pillared structures include many types of phosphonates [3], sulfates [4], and molybdates [5] as well as heterometallic solids that incorporate additional transition metals for preferentially bonding to the bridging organic ligands [5–7]. The late transition-metal cations can be of a wide variety (e.g. Cu^{2+}, Ni^{2+}, Co^{2+}, Fe^{2+}) and are incorporated into the layer via coordination to the intralayer anions (PO_4^{3-}, MoO_4^{2-}, etc.). Thus, a significant diversity of layered pillared solids is possible by using a variety of transition metals and/or pillaring ligands, with some recent examples including $[Cu(4,4'\text{-bipyridine})_{0.5}MoO_4]\cdot 1.5H_2O$ [8], $[Cu(tripyridyltriazine)_2Mo_4O_{13}]$ [6], $[Co_3(pyrazine)(HPO_4)_2F_2]$ [9], and $[Cu(4,4'\text{-dipyridylamine})VO_3]$ [7]. In these examples, the metal-oxide layer and the bridging organic ligand are formally neutral, but the removal of these pillaring molecules at relatively low temperatures has usually not been investigated.

The utilization of Ag-containing oxide layers within the context of organic-pillared solids remains relatively unexplored. Among Ag-containing heterometallic oxides, potential applications include carbon monoxide oxidation

*Corresponding author. Fax: +1 919 515 5079.
E-mail address: Paul_Maggard@ncsu.edu (P.A. Maggard).

0022-4596/$ - see front matter © 2005 Elsevier Inc. All rights reserved.
doi:10.1016/j.jssc.2005.10.037

($AgCoO_2/Co_3O_4$, Ag_2O/γ-Mn_2O_3 composites, σ-$AgFeO_2$) [10–12], oxidative dehydrogenation of propane ($AgMoO_2PO_4$) [13], as well as other oxidative reactions [14]. Synthesis of pillared heterometallic-organic/oxides containing silver would hold promise for studying catalytic reactions whereby the guest molecules (such as CO) could be incorporated within the micropores. Or alternatively, heterometallic-organic/oxides that are pillared by easily removable ligands could potentially serve as useful precursors to new condensed oxides, with the resultant structure deriving from the condensation of the purely inorganic layers. In our group, prior research efforts on pillared solids have demonstrated that the parent $AgReO_4$ solid can be pillared by metal-coordinated bridges, e.g. in $M(pzc)_2(H_2O)_2$ (M = Co, Ni; pzc = pyrazinecarboxylate) to give $M(pzc)_2(H_2O)_2AgReO_4$ [15] or in $Cu(pzc)_2$ to give the chiral $Cu(pzc)_2AgReO_4$ [16]. In these examples, the neutral water ligands that are coordinated to the axial sites of the $M(pzc)_2$ pillar can be reversibly removed without the loss of the structure crystallinity to generate coordinatively unsaturated metal sites, while the chelating pyrazinecarboxylate ligand is removed at higher temperatures (>300 °C) and can effect changes in the layer composition owing to its charge. These three reported structures can be viewed as derived from the $AgReO_4(pyz)$ (pyz = pyrazine) structure, reported herein, whereby the pyrazine ligand has been substituted for with metal-coordinated pillars, i.e. $M(pzc)_2(H_2O)_2$. Thus, the syntheses of pyrazine-pillared structures can be used to help forecast future structures and compositions based on the substitutions of different organic pillars, such as for $Ag_3Mo_2O_4F_7(pyz)_3$ described below.

Presented herein is the synthesis, structure and physical properties of two new pyrazine-pillared structures, $AgReO_4(C_4H_4N_2)$ (**I**) and $Ag_3Mo_2O_4F_7(C_4H_4N_2)_3$ ($C_4H_4N_2$ = pyrazine, pyz) (**II**), which have been characterized for ligand loss during thermogravimetric analysis, and also for their optical properties including photoluminescence and UV-Vis diffuse reflectance. The optical properties are analyzed with respect to the calculated electronic band structure and also to that exhibited by previously reported inorganic counterparts.

2. Experimental

Caution: Hydrofluoric acid is toxic and corrosive!

Materials: Ag_2O (99%, Aldrich), MoO_3 (99.9995%+, Alfa Aesar), Re_2O_7 (99.9%+, Alfa Aesar), pyrazine (99+%, Aldrich), HCl (aqueous, 37.4% Fisher) and HF (aqueous, 49% Aldrich) were used as received. Reagent amounts of deionized water were also used in the synthesis.

Synthesis: The synthesis of $AgReO_4(pyz)$ was performed by adding 2.09×10^{-1} g (4.32×10^{-4} mol) of Re_2O_7, 1.00×10^{-1} g (4.32×10^{-4} mol) of Ag_2O, 6.91×10^{-2} g (8.63×10^{-4} mol) of pyrazine, and 6.22×10^{-1} g (3.45×10^{-2} mol) of H_2O to an FEP Teflon pouch. The pouch was heat sealed and placed inside a 125 mL Teflon-lined stainless steel reaction vessel that was backfilled with ~42 mL deionized H_2O before closing. The reaction vessel was heated to 150 °C for 24 h inside a convection oven and slowly cooled to room temperature at 6 °C h^{-1}. Colorless bar-shaped crystals were recovered by filtration in ~85% yield based on silver. Large (mm-sized) octahedral $AgReO_4$ crystals also formed as a side product. Hydrothermal reactions at lower temperatures (e.g. 120 °C) did not result in higher yield or purity of the product. However, $AgReO_4(pyz)$ could be synthesized in high purity from a hydrothermal reaction of $AgReO_4$ and pyrazine at 150 °C for 24 h, resulting in only large transparent crystals of the product. The crystals were extracted manually from the latter for subsequent physical property measurements.

The synthesis of $Ag_3Mo_2O_4F_7(pyz)_3$ was performed analogous to the procedures above, by reacting 2.41×10^{-1} g (1.67×10^{-3} mol) of MoO_3, 5.82×10^{-1} g (2.51×10^{-3} mol) of Ag_2O, 6.71×10^{-2} g (8.38×10^{-4} mol) of pyrazine, 5.94×10^{-1} g (1.68×10^{-2} mol) of 49% aqueous HF and 1.56×10^{-2} g (6.28×10^{-4} mol) of concentrated HCl in an FEP teflon pouch that was placed inside a 125 mL Teflon-lined stainless steel reaction vessel and 1/3 backfilled with deionized H_2O. HCl is necessary to grow high-purity crystals, although the chloride ion itself does not go into the structure. The reaction vessel was heated to 150 °C for 24 h inside a convection oven and slowly cooled to room temperature at 6 °C h^{-1}. Yellow needle- and tubular-shaped crystals were recovered by filtration in ~75% yield based on silver.

Crystallographic structure determination: Several bar-shaped and transparent crystals of $AgReO_4(pyz)$ were examined under an optical microscope equipped with cross polarizers, and were mounted for data collection on a Bruker CCD diffractometer operating at 110 K. The unit cell obtained was monoclinic with $a = 7.2238(6)$ Å, $b = 7.4940(7)$ Å, $c = 15.451(1)$ Å, and $\beta = 92.296(4)°$. One-half sphere of reflections ($\pm h,k,l$) was collected and processed with SAINTPLUS [17] to $2\theta = 72.85°$ to give 47921 reflections, of which 3825 were unique and observed ($F > 1\sigma_F$). The structure was solved and refined using SHELXTL [18] in the monoclinic space group $P2_1/c$ (No. 14) and checked for additional symmetry elements using the program PLATON [19]. Hydrogen atoms on the pyrazine molecules were refined in idealized positions at a C–H distance of 0.96 Å. Final anisotropic structure refinement converged at $R_1/wR_2 = 0.039/0.050$ ($R_{ave} = 0.033$), with a data:variable ratio of ~35:1. The highest residual electron density peak was 1.47 e $Å^{-3}$.

Yellow-colored needle crystals of $Ag_3Mo_2O_4F_7(pyz)_3$ were characterized according to similar procedures as outlined above, with the procedure modifications described below. A single crystal was selected and fixed on a glass fiber using epoxy and centered on an Enraf-Nonius CAD4-MACH diffractometer operating at 148 K. The unit cell was determined by a fit of 25 well-centered reflections in the range of $34° < 2\theta < 36°$, and was measured to be monoclinic with $a = 7.6465(9)$ Å, $b = 7.1888(5)$ Å, $c = 19.142(2)$Å, and

Table 1
Selected crystal and refinement data for $AgReO_4(C_4H_4N_2)$ (**I**) and $Ag_3Mo_2O_4F_7(C_4H_4N_2)_3$ (**II**)

Compound	I	II
Fw	438.16	952.72
Space group, Z	$P2_1/c$ (No. 14), 4	$P2/n$ (No. 13), 2
T (K)	110	148
a (Å)	7.2238(6)	7.6465(9)
B	7.4940(7)	7.1888(5)
C	15.451(1)	19.142(2)
β	92.296(4)	100.284(8)
V	835.8(1)	1035.3(2)
μ (Mo$K\alpha$) (mm^{-1})	16.79	4.05
d_{calc}, ($g\,cm^{-3}$)	3.48	3.06
Reflections (total), R_{int}	47921	3630
Data/restraints/parameters	3815/0/109	1777/0/157
Final R_1, wR_2[a] [$I>2\sigma(I)$]	0.039, 0.050	0.025, 0.037

[a] $R_1 = \Sigma||F_o|-|F_c||/\Sigma|F_o|$; $wR_2 = \{\Sigma[w(F_o^2-F_c^2)^2]/\Sigma[w(F_o^2)^2]\}^{1/2}$, $w = \sigma_F^{-2}$.

$\beta = 100.284(8)^\circ$. Two octants of data were collected ($\pm h, +k, +l$) twice (i.e. a redundant data set), to give a total of 3630 reflections of which 1777 were unique and observed ($F>1\sigma_F$). Three standard reflections were measured every 80 min of X-ray exposure time to monitor and correct for crystal decomposition. Data reduction utilized routines from the NRCVAX suite of programs [20], and the structure was solved using SIR92 [21] in the monoclinic space group $P2/n$ (No. 13). Final anisotropic structure refinement converged at $R_1/wR_2 = 0.025/0.037$ ($R_{ave} = 0.040$) with a data:variable ratio of ~11:1. The highest residual electron density peak was $1.16\,e\,Å^{-3}$ (and $-1.30\,e\,Å^{-3}$).

Some data collection and refinement parameters for both solids, as well as selected atomic coordinates and isotropic-equivalent displacement parameters are listed in Tables 1–3. Interatomic contacts for selected bonds in both

Table 2
Selected atomic coordinates and equivalent isotropic displacement parameters ($Å^2$) for $AgReO_4(C_4H_4N_2)$

Atom	Wyckoff letter	x	y	z	U(eq)[a]
Re	4e	0.47856(2)	0.84442(2)	0.61992(1)	0.02696(9)
Ag	4e	0.47852(4)	0.63526(5)	0.36809(2)	0.0266(1)
O1	4e	0.2537(6)	0.9190(7)	0.6169(3)	0.060(3)
O2	4e	0.6247(7)	0.0228(6)	0.6139(3)	0.059(3)
O3	4e	0.5065(6)	0.7066(5)	0.5330(2)	0.044(2)
O4	4e	0.5263(6)	0.7251(6)	0.7134(2)	0.043(2)
N1	4e	0.7861(4)	0.6089(5)	0.3704(2)	0.026(2)
N2	4e	0.1701(4)	0.6082(5)	0.3686(2)	0.027(2)
C1	4e	0.8778(5)	0.5208(6)	0.3092(3)	0.030(2)
C2	4e	0.0688(5)	0.5224(6)	0.3085(3)	0.031(2)
C3	4e	0.0815(6)	0.6956(6)	0.4300(3)	0.030(2)
C4	4e	0.8896(6)	0.6947(6)	0.4305(3)	0.030(2)

[a] U(eq) is defined as one-third of the trace of the orthogonalized U_{ij} tensor.

Table 3
Selected atomic coordinates and equivalent isotropic displacement parameters ($Å^2$) for $Ag_3Mo_2O_4F_7(C_4H_4N_2)_3$

Atom	Wyckoff letter	x	y	z	U(eq)[a]
Ag1	4g	0.82352(3)	0.44824(4)	0.43178(1)	0.0126(2)
Ag2	2f	0.75	0.50221(5)	0.25	0.0130(2)
Mo	4g	0.69194(4)	0.51726(4)	0.63963(2)	0.0105(2)
F1	2f	0.75	0.5959(4)	0.75	0.013(1)
F2	4g	0.6786(2)	0.7825(3)	0.6248(1)	0.017(1)
F3	4g	0.9513(2)	0.5598(3)	0.6524(1)	0.017(1)
F4	4g	0.7541(3)	0.2751(3)	0.6762(1)	0.0174(9)
O1	4g	0.6720(3)	0.4558(4)	0.5525(2)	0.019(1)
O2	4g	0.4718(3)	0.5023(3)	0.6527(1)	0.013(1)
N1	4g	0.8319(3)	0.7550(5)	0.4351(1)	0.011(1)
N2	4g	0.8194(3)	0.1421(4)	0.4303(1)	0.011(1)
N3	2f	0.75	0.1952(6)	0.25	0.010(2)
N4	2f	0.75	0.8087(6)	0.25	0.009(2)
C1	4g	0.6941(4)	0.8495(5)	0.4523(2)	0.013(2)
C2	4g	0.6885(5)	0.0409(5)	0.4494(2)	0.013(2)
C3	4g	0.9549(4)	0.0480(5)	0.4112(2)	0.011(2)
C4	4g	0.9609(4)	0.8540(5)	0.4138(2)	0.011(2)
C5	4g	0.6079(4)	0.0975(5)	0.2622(2)	0.011(1)
C6	4g	0.6084(4)	−0.0955(5)	0.2625(2)	0.011(2)

[a] U(eq) is defined as one-third of the trace of the orthogonalized U_{ij} tensor.

Table 4
Selected interatomic distances (Å) and angles (deg) in $AgReO_4(C_4H_4N_2)$ (**I**) and $Ag_3Mo_2O_4F_7(C_4H_4N_2)_3$ (**II**)

Atom 1	Atom 2	Mult.	Distance	Intra-polyhedral angles		
I						
Ag1	N1		2.229(3)	Re	O1	1.717(4)
	N2		2.238(3)		O2	1.708(4)
	O2		2.686(5)		O3	1.713(3)
	O3		2.603(3)		O4	1.722(4)
	O4		2.644(3)			
II						
Ag1	N1		2.207(3)	Mo	O1	1.705(3)
	N2		2.201(3)		O2	1.749(2)
	O1		2.765(3)		F1	2.1552(8)
	O2		2.557(3)		F2	1.928(2)
	F3		2.560(2)		F3	1.978(2)
					F4	1.904(2)
Ag2	N3		2.207(4)			
	N4		2.203(4)			
	O2	2 ×	2.733(2)			
	F3	2 ×	2.718(2)			

solids are given in Table 4. Included in the supporting information is a complete list of data collection, refinement and anisotropic displacement parameters and all near-neighbor interatomic distances.

Optical property measurements: Approximately 50 mg of powder of each sample was mounted onto a fused-silica holder and placed along the external window of an integrating sphere inside a Cary 300 spectrophotometer to measure the UV-Vis diffuse reflectance spectra (DRS). Pressed polytetrafluoroethylene powder was used as a reference and the data were plotted as the remission function $F(R_\infty) = (1-R_\infty)^2/(2R_\infty)$, where R is diffuse reflectance based on the Kubelka–Monk theory of diffuse reflectance. Emission and excitation spectra were measured with an ISS PC-1 fluorometer equipped with a Xenon arc lamp using front face detection geometry to orient the sample face at an angle of 22.5° with respect to the incident beam. A low band-pass UG-11 filter was placed after the excitation monochromator. Excitation spectra were corrected by a rhodamine-B quantum counter and emission spectra were corrected with respect to a standard quinine sulfate solution and a NIST spectrum.

Thermogravimetric analyses: Weighed samples of 31.79 of **I** and 32.81 mg of **II** were loaded onto Pt pans, equilibrated and tarred at room temperature, and heated at a rate of 1 °C min^{-1} for **I** or 0.5 °C min^{-1} for **II** to 400 °C under flowing nitrogen on a TA Instruments TGA Q50.

Electronic band structure calculations: Extended Hückel calculations were carried out within the tight-binding approximation, using the CAESAR2 program [22], for the full structures of **I** and **II** at 960 k-points spread over the irreducible wedge. The double zeta basis sets were selected for the atomic orbital parameters, and the atomic coordinates and lattice dimensions were taken from the respective single crystal structures.

3. Results and discussion

Structural descriptions. $AgReO_4(pyz)$ (I): Colorless crystals of **I** are comprised of neutral $AgReO_4$ layers that are bridged via pyrazine ligands to the Ag sites in each layer, as shown in Fig. 1. The single symmetry-unique layer stacks directly above and below, down the a-axis, to generate the full 3D structure. The shortest interlayer spacing is set by the length of the pyrazine ligand at 2.78 Å, while the ReO_4 tetrahedra, which line the spaces between the Ag(pyz) pillars, are separated at a distance of 4.61 Å (O1–O2) across the individual layers (marked). Each ReO_4 tetrahedron bonds via three O vertices to three different Ag^+ in the layer (Ag–O of 2.603(3)–2.686(5) Å), with the fourth vertex either above or below the layer, as shown in Fig. 2. The symmetry-unique atoms and distances are labeled in Fig. 2B and listed in Table 4. Each Ag^+ is bonded to the three oxide groups from the three separate ReO_4 tetrahedra as well as to the nitrogen groups on two pyrazine ligands above and below each layer, at 2.229(3) Å and 2.238(3) Å for Ag1–N1 and –N2, respectively, similar to that in related silver-pyrimidine networks [23].

Related but nondistorted $AgReO_4$ layers can be found in the [110] planes of the 'organic-free' $AgReO_4$ crystal structure [24], with however a different rotational arrangement of all of the ReO_4 tetrahedra. Roughly, the arrangement of cations and anions within the $AgReO_4$ layer of both solids has each Ag^+ surrounded by four ReO_4^- groups (though with the fourth separated at a larger distance in $AgReO_4(pyz)$), and with each ReO_4^- group similarly bordered by four Ag^+ cations. Thus, the layers of **I** can be viewed as sections of the [110] planes in $AgReO_4$ that have been cleaved and pillared by bridging pyrazine ligands. However, fairly narrow ellipsoidal areas are formed as a result of the structural changes in each layer in $AgReO_4(pyz)$, Fig. 2B, that are approximately 3 Å × 12 Å (from O3 to O3 or O4–Ag1 and O2–O2). The thermal displacement parameters of Ag do not indicate any preferential displacements into this area.

$Ag_3Mo_2O_4F_7(pyz)_3$ (II): The yellow-needle crystals of **II** are comprised of neutral $Ag_3Mo_2O_4F_7$ layers that are bridged via pyrazine ligands that bond to Ag sites in each layer, as illustrated in Fig. 3. The pyrazine-pillared molybdate layers stack directly above and below to generate the full 3D structure. The shortest interlayer spacing is set by the length of the pyrazine ligand at 2.78 Å, while $Mo_2O_4F_7^{3-}$ dimers border the 'open' areas between the layers, together with the sets of three edge-shared Ag(pyz) chains, and are separated at a shortest distance of 3.69 Å ($F2$–$F4$) across the layers. Only the fluoride atoms of $Mo_2O_4F_7^{3-}$ project between the layers, while the oxide groups bond to Ag^+ in the plane of the layers.

Structural views normal to the individual layers of **II** are shown in Fig. 4, either as polyhedra (4A) or with the

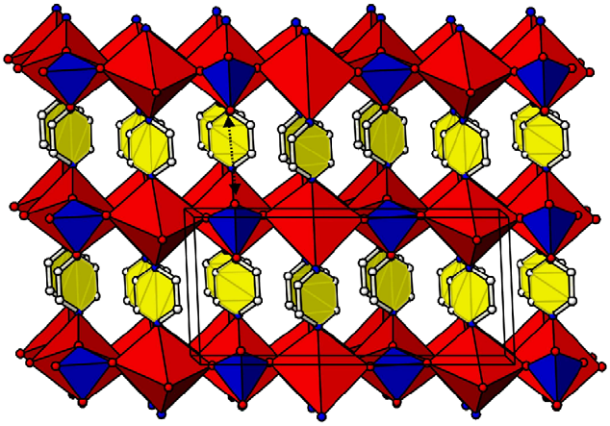

Fig. 1. A ~[010] polyhedral view of the $AgReO_4(pyz)$ structure with the unit cell outlined. Red polyhedra are Ag-centered coordination environments and blue polyhedra are ReO_4.

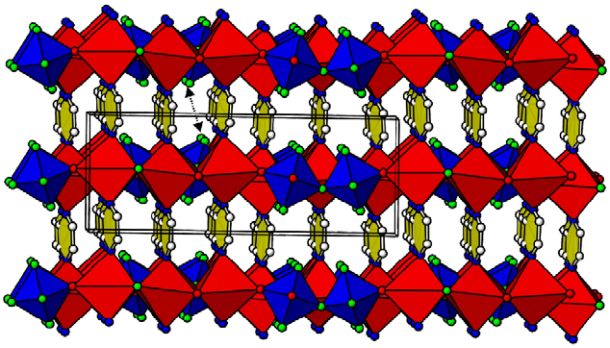

Fig. 3. An ~[010] edge-on view of the pyrazine-bridged layers in $Ag_3Mo_2O_4F_7(pyz)_3$. Both the unit cell and the shortest interlayer F–F distance are marked. Red polyhedra are Ag-centered, blue are Mo-centered and yellow are pyrazine molecules.

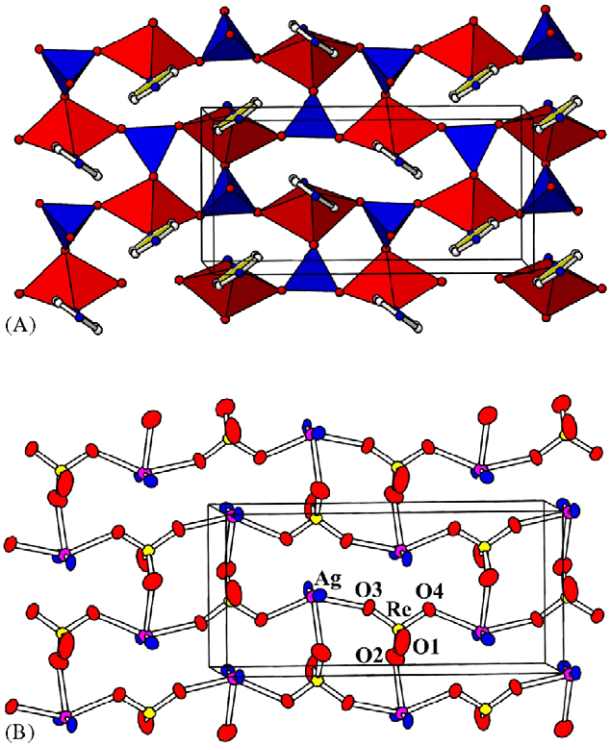

Fig. 2. Structural views of a single $AgReO_4$ layer drawn using (A) metal-centered polyhedra and (B) 80% probability thermal ellipsoids. Symmetry unique atoms are labeled in B, where red ellipses are O, blue are N, yellow are Re, and purple are Ag.

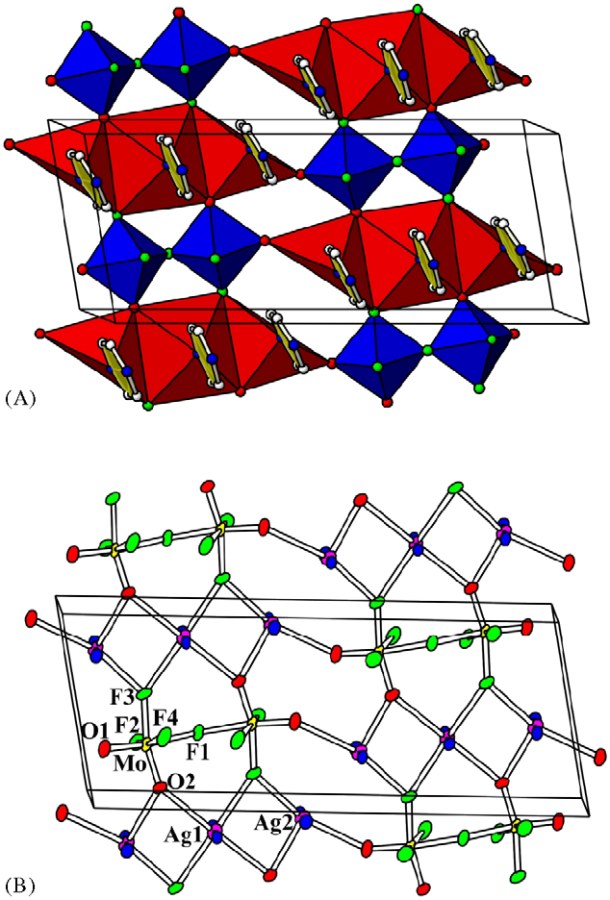

Fig. 4. Structural views of a single $Ag_3Mo_2O_4F_7$ layer drawn using (A) metal-centered polyhedra and (B) 80% probability thermal ellipsoids. Symmetry unique atoms are labeled in B, where red ellipses are O, blue are N, green are F, yellow are Mo, and purple are Ag.

symmetry-unique atoms labeled (4*B*). Selected interatomic distances are listed in Table 4. The $Mo_2O_4F_7^{3-}$ dimer is the first known example of a vertex-shared octahedral dimer among oxyfluoride molybdates, although evidence for the formation of vertex-shared tetrahedra in $Mo_2O_2F_9^-$ in solution and $W_2O_4F_7^{3-}$ in $Cs_3[W_2O_4F_7]$ were both reported some time ago [25,26]. The $Mo_2O_4F_7^{3-}$ dimer can be viewed as a condensation of two $MoO_2F_4^{2-}$ octahedra via an F vertex, with the Mo atoms displaced towards the two nearest *cis*-O groups. The Mo–O and –F distances are regular and fall within the expected ranges [27], with two short *cis*-O distances of 1.705(3) Å and 1.749(2) Å (Mo–O1 and Mo–O2) and four longer F distances of 1.904(2)–2.1552(8)Å (Mo–F4 to Mo–F1). Each $Mo_2O_4F_7^{3-}$ dimer bonds via the four O vertices to Ag^+ in the plane of

the layer (Ag1–O1 and –O2 of 2.765(3) Å and 2.557(3) Å; Ag2–O2 of 2.733(2)'Å, ×2), and also via two F atoms to the Ag^+ sites (Ag1–F3 of 2.560(2) Å and Ag2–F3 of 2.718(2) Å, ×2). As a result, sets of edge-shared rows of three Ag^+ each share O/F vertices to two sets of molybdate dimers, with one vertex missing on Ag1. Each Ag is additionally coordinated to pyrazine ligands both above and below (Ag1–N1 and –N2 at 2.207(3) Å and 2.201(3) Å; Ag2–N3 2.207(4) Å and 2.203(4) Å) that bridges to adjacent layers.

Between the layers the pyrazine groups arrange face-to-face at a $\pi-\pi$ stacking distance of ~3.5 Å, which is within the ranges of π–π interaction distances reported previously [28,29]. The close $\pi-\pi$ interactions are formed as a result of the sets of three edge-shared Ag^+ cations in **II**, whereas close $\pi-\pi$ interactions and near neighbor Ag^+ cations are both absent in **I**. The arrangement of cations and anions within each layer has a NaCl-type repeating pattern, with each set of three Ag^+ cations surrounded by four $Mo_2O_4F_7^{3-}$ dimers, and conversely each $Mo_2O_4F_7^{3-}$ is surrounded by four sets of three Ag^+ cations.

Thermogravimetric analysis (*TGA*): The thermal stability of **I** and **II** were investigated by heating each sample to 400 °C under flowing N_2. Shown in Fig. 5, the TGA of **I** displayed a weight-loss step of 17% extending from ~150 to 175 °C that corresponded to the loss of pyrazine ligands (theoretical weight loss—18%). The silvery-white product formed from heating **I** was determined to be crystalline $AgReO_4$ by powder X-ray diffraction. Further weight loss or change in structure up to 400 °C was not observed. The TGA of **II** up to 400 °C showed a single weight-loss step of 33% extending from ~150 to 200 °C, corresponding to a weight loss 8% greater than that expected by the loss of pyrazine alone (theoretical weight loss—25%). A powder X-ray diffraction of the deep red product obtained from the TGA analysis corresponded to Ag_2MoO_4 as well as containing some unidentified peaks. The origin of the additional weight loss is undetermined, but it would correspond to a loss of half of the original O/F atoms, such as could occur in a reaction with the ligand to give, for example, CO or CO_2. Both solids begin to decompose at a temperature only somewhat higher than their preparation temperature (150 °C), illustrating the ease with which the pyrazine ligands can be removed, and which also shows pyrazine-pillared phases could hold promise as useful low temperature precursors to condensed oxides, i.e. as shown for $AgReO_4$ and Ag_2MoO_4 here.

Optical properties and electronic structure calculations: As both solids are two-dimensional versions of insulating/semiconducting metal oxides, the optical band gaps and photoluminescent properties were measured to analyze the resultant effects of pillaring and reduced dimensionality. The UV-Vis DRS of **I** ($AgReO_4$(pyz)) is plotted in Fig. 6, and exhibits an optical absorption edge in the near ultraviolet with an estimated optical band gap of 2.91 eV. In the case of 'organic-free' $AgReO_4$, this excitation reportedly arises from a metal-to-metal charge transfer from Ag^+ to Re^{7+} (i.e. $Ag^{I}Re^{VII} \rightarrow Ag^{III}Re^{V}$) at a relatively blue-shifted energy of 3.7 eV, but which decreases with increasing pressure at a rate of ~80 meV GPa^{-1} [30]. Significantly, this MMCT in $AgReO_4$ also results in an orange photoluminescence at 580 nm owing to the photo-emissive triplet state on silver [31]. This photoluminescence is also expressed here in the pillared structure of **I** at a slightly different wavelength of 575 nm, shown in Fig. 7. However, the Ag^+ cations in **I** have farther spaced ReO_4 neighbors (and different orientations) than in the simpler $AgReO_4$, and are also coordinated covalently to the pyrazine ligands. To probe the nature of this electronic transition in $AgReO_4$(pyz), electronic structure calculations were performed and the densities of states (DOS) plotted in Fig. 8. The partial DOS have been projected out for each element type, and show a predominance of states arising from Re (unfilled) and Ag (filled) both above and below the band gap, as found in $AgReO_4$ as expected for a

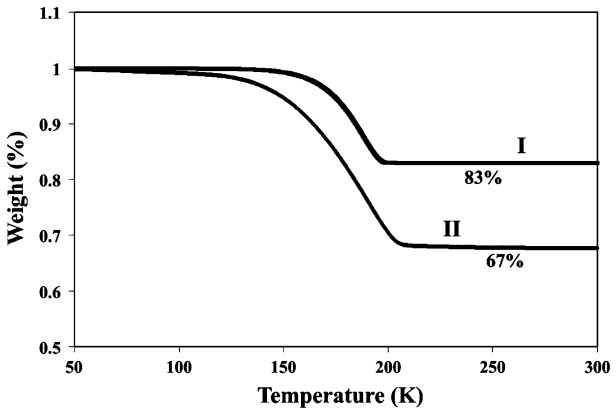

Fig. 5. Thermogravimetric curves for **I,** $AgReO_4$(pyz), and **II**, $Ag_3Mo_2O_4F_7(pyz)_3$, with the value at each temperature calculated as percent of the original weight.

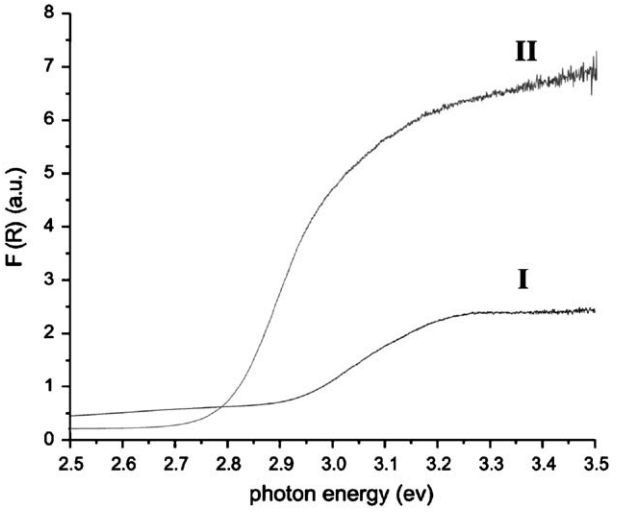

Fig. 6. A plot of UV-Vis diffuse reflectance spectra, F(R) vs. photon energy (eV), for $AgReO_4$(pyz) (**I**) and $Ag_3Mo_2O_4F_7(pyz)_3$ (**II**).

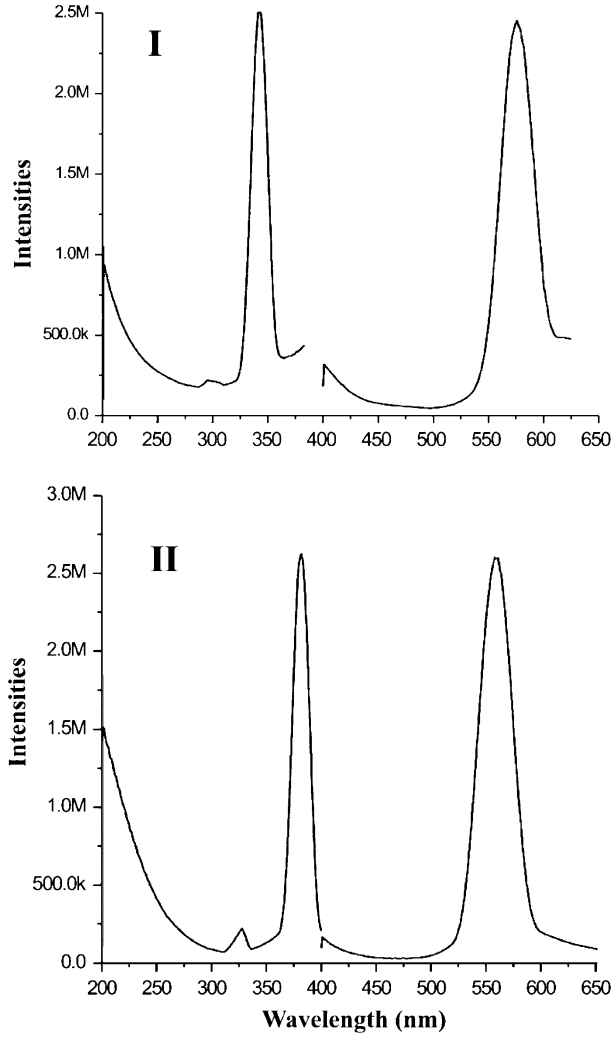

Fig. 7. Electronic excitation (left curve) and emission (right curve) spectra of $AgReO_4(pyz)$ (**I**) and $Ag_3Mo_2O_4F_7(pyz)_3$ (**II**).

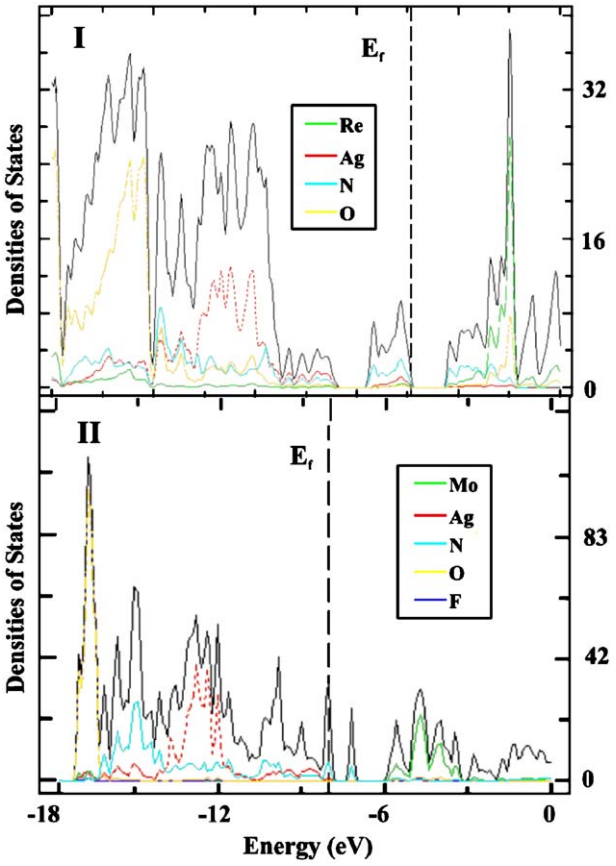

Fig. 8. Calculated electronic densities of states (DOS) for $AgReO_4(pyz)$ (**I**) and $Ag_3Mo_2O_4F_7(pyz)_3$ (**II**), with projections of partial densities of states for each element.

metal-to-metal charge transfer [32]. However, owing to the addition of pyrazine to the structure, additional states arising from the ligand (C and N) are located at just below and also ~0.8 eV above the Fermi level, and allows the possibility of photoemissive excited states arising from a ligand charge transfer instead. The ~0.8 eV smaller band gap in the pyrazine-pillared structure, though with an energetically similar photoluminescence as $AgReO_4$, could suggest a different electronic origin.

The UV-Vis DRS of **II** ($Ag_3Mo_2O_4F_7(pyz)_3$), plotted in Fig. 6, exhibits an optical absorption edge in the visible region with an estimated optical band gap of 2.76 eV. The smaller visible-region band gap of **II** is confirmed by its yellow color, compared to crystals of **I** which are transparent and colorless. This lowest-energy optical absorption arises in 'organic-free' molybdates from a ligand-to-metal charge transfer (LMCT) between O^{2-} and Mo^{6+}, to yield short-lived (transient) Mo^{5+} and O^- sites. The energy of this transition is typically ~2.81 eV for related molybdates [33] and which is close to that for **II** here. Shown in Fig. 7, a strong photoluminescent emission was also observed for **II** at $\lambda = 580$ nm with a maximum excitation at $\lambda = 380$ nm. Photoluminescence of a related oxyfluoromolybdate, $CdMoO_3F_2$ [34], arises from the same type of LMCT and occurs at $\lambda = 660$ nm, which is significantly red-shifted compared to **II**. In order to investigate the type of lowest-energy electronic transition in $Ag_3Mo_2O_4F_7(pyz)_3$, electronic structure calculations were performed and the DOS) plotted in Fig. 8. In analogy to that for **I**, the partial DOS have been projected out for each element type, and show the predominant number of states both above and below the Fermi level arise from filled Ag (higher energies) and O (lower energies)-based states and empty Mo-based states. These results suggest an MMCT transition (i.e. $Ag^{I}Mo^{VI} \rightarrow Ag^{III}Mo^{IV}$), similar to that in $AgReO_4(pyz)$, is lower in energy and likely favored over the higher energy LMCT transition. Thus, it is expected that both **I** and **II** exhibit nearly energetically similar photoemissions (560 vs. 575 nm) arising from the photoemissive excited states on silver in both cases. However, a small amount of additional states arise from the pyrazine ligands (C and N) at just below and above the Fermi level that could also act as excited-state (π^*)

acceptors, such as found similarly in the DOS for **I**. The effect of the pyrazine pillars in the electronic structures of **I** and **II** is the introduction of additional pyrazine-based states near the Fermi level, and suggests a similar origin of their photoluminescence that is related but different to that found in $AgReO_4$.

4. Conclusions

As part of research efforts to uncover new layered solids, two new pillared hybrid structures containing Ag(pyz) chains were synthesized under hydrothermal conditions, $AgReO_4(pyz)$ and $Ag_3Mo_2O_4F_7(pyz)_3$. The pyrazine-bridged layers in $AgReO_4(pyz)$ are analogous to the [110] planes of layers in the simpler $AgReO_4$ compound, with a different orientation of the ReO_4 tetrahedra. The octahedral $Mo_2O_4F_7^{3-}$ dimers in $Ag_3Mo_2O_4F_7(pyz)_3$ share vertices with sets of three edge-shared $Ag(pyz)^+$ chains that form $\pi-\pi$ stacked pillars. In both the pyrazine pillars are removed at temperatures slightly higher than the preparation temperature, with a full loss of ligand that results in crystalline $AgReO_4$ for **I** and Ag_2MoO_4 and an unidentified product for **II**. Both pyrazine-pillared solids exhibit photoluminescence likely arising in both from a charge transfer excitation (MMCT or LMCT) and photoemission that is analogous to that reported for $AgReO_4$. The synthesis of future pillared structures that are microporous and photoluminescent would hold promise for small molecule detection as well as for probing the fundamental chemical origins of the optical properties of the layers.

Supporting information available: Powder X-ray diffraction data for post-TGA products for **I** and **II**. Crystallographic data (excluding structure factors) for the structure(s) reported in this paper have been deposited with the Cambridge Crystallographic Data Centre as supplementary publication no. CCDC 252350 & 252351. Copies of the data can be obtained free of charge on application to CCDC, 12 Union Road, Cambridge CB2 1EZ, UK (fax: (44) 1223 336-033; e-mail: deposit@ccdc.cam.ac.uk).

Acknowledgments

P.M. acknowledges support from NCSU for startup funds, from the ACS-PRF (#40963-G10), and from the Beckman Foundation as a Beckman Young Investigator. The authors thank C. Stern for the single crystal X-ray data of **I**, Digamber Porob for help with powder X-ray diffraction data, and Jaap Folmer for use of the TGA. The authors acknowledge support from the National Science Foundation (NSF) for funding (Award No. 9509532) to purchase the X-ray diffractometer.

Appendix A. Supplementary data

Supplementary data associated with this article can be found in the online version at doi:10.1016/j.jssc.2005.10.037.

References

[1] (a) M.S. Whittingham, A.J. Jacobson (Eds.), Intercalation Chemistry, Academic Press, New York, 1982;
(b) D. O'Hare, Inorganic intercalation compounds, in: D.W. Bruce, D. O'Hare (Eds.), Inorganic Materials, Wiley, Chichester, 1996.
[2] (a) M. Morcrette, P. Rozier, L. Dupont, E. Mugnier, L. Sannier, J. Galy, J.-M. Tarascon, Nature Mater. 2 (2003) 755–761;
(b) M. Kondo, T. Okubo, A. Asami, S.-I. Noro, T. Yoshitomi, S. Kitagawa, T. Ishii, H. Matsuzaka, K. Seki, Angew. Chem. Int. Ed. 38 (1/2) (1999) 140–143;
(c) E.M. Serwicka, K. Bahranowski, Catal. Today 90 (1–20) (2004) 85–92.
[3] A. Clearfield, Chem. Mater. 10 (1998) 2801–2810.
[4] A.P. Cote, K. George, H. Shimizu, Chem. Commun. 3 (2001) 251–252.
[5] P.J. Hagrman, D. Hagrman, J. Zubieta, Angew. Chem. Int. Ed. 38 (1999) 2638–2684.
[6] D.E. Hagrman, J. Zubieta, J. Solid State Chem. 152 (2000) 141–151.
[7] R.L. LaDuca, R. Finn, J. Zubieta, Chem. Commun. (1999) 1669–1670.
[8] R.S. Rarig, R. Lam, P.Y. Zavalij, J.K. Ngala, R.L. LaDuca, J.E. Greedan, J. Zubieta, Inorg. Chem. 41 (8) (2002) 2124–2133.
[9] W.-K. Chang, R.-K. Chiang, Y.-C. Jiang, S.-L. Wang, S.-F. Lee, K.-H. Lii, Inorg. Chem. 43 (8) (2004) 2564–2568.
[10] C. Guelder, React. Kin. Catal. Lett. 78 (1) (2003) 161–168.
[11] W.-P. Liu, Y.-J. Zhong, M.-F. Luo, React. Kin. Catal. Lett. 72 (2) (2001) 289–295.
[12] (a) E. Gulari, C. Gulder, S. Srivannavit, S. Osuwan, Appl. Catal. A 182 (1) (1999) 147–163;
(b) M. Chen, M. Luo, X. Zheng, Yingyong Huaxue 16 (1) (1999) 50–53.
[13] X. Zhang, H.L. Wan, W.Z. Weng, X.D. Yi, Chin. Chem. Lett. 13 (9) (2002) 907–910.
[14] M. Chen, M. Luo, X. Zheng, Yingyong Huaxue 16 (1) (1999) 50–53.
[15] P.A. Maggard, B. Yan, J. Luo, Angew. Chem. Int. Ed. 44 (2005) 2553–2556.
[16] B. Yan, M.D. Capracotta, P.A. Maggard, Inorg. Chem. 44 (2005) 6509–6511.
[17] SAINTPLUS Bruker, AXS, Inc., Madison, WI, 1997.
[18] G.M. Sheldrick, SHELXTL Programs, Version 5.1, Bruker AXS, Inc., Madison, WI, 1998.
[19] A.L. Spek, PLATON, Utrecht University, Utrecht, The Netherlands, 2001.
[20] E.J. Gabe, Y. Le Page, J.P. Charland, F.L. Lee, P.S. White, J. Appl. Crystallogr. 22 (4) (1989) 384–387.
[21] A. Altomare, G. Cascarano, C. Giacovazzo, A. Guagliardi, J. Appl. Crystallogr. 26 (3) (1993) 343–350.
[22] M.-H. Whangbo, CAESAR, Department of Chemistry, North Carolina State University, Raleigh, NC, 1998.
[23] C.V. Krishnamohan Sharma, S.T. Griffin, R.D. Rogers, Chem. Commun. (1998) 215–216.
[24] F. Buschendorf, Z. Physik. Chem. B 20 (1933) 237–244.
[25] Y.A. Buslaev, Y.V. Kokunov, V.A. Bochkareva, E.M. Shustorovich, Zhurn. Strukt. Khimii 13 (3) (1972) 526–528.
[26] R. Mattes, H. Foerster, Z. Anorg. Allg. Chem. 494 (1982) 109–114.
[27] P.A. Maggard, A.L. Kopf, C.L. Stern, K.R. Poeppelmeier, K.M. Ok, P.S. Halasyamani, Inorg. Chem. 41 (19) (2002) 4852–4858.

[28] S.V. Eliseeva, O.V. Mirzov, S.I. Troyanov, A.G. Vitukhnovsky, N.P. Kuzmina, J. Alloys Compds. 374 (1–2) (2004) 293–297.
[29] K. Sakai, M. Kurashima, Acta Crystallogr. Sect. E E59 (7) (2003) m411–m413.
[30] J.W. Otto, J.K. Vassiliou, R.F. Porter, A.L. Ruoff, J. Phys. Chem. Solids 53 (5) (1992) 631–638.
[31] H. Kunkely, A. Vogler, Inorg. Chim. Acta 357 (2004) 1317–1319.
[32] J. Spitaler, C. Ambrosch-Draxl, E. Nachbaur, F. Belaj, H. Gomm, F. Netzer, Phys. Rev. B 27 (2003) 115127(-1)–115127(-9).
[33] T. Yamase, H. Naruke, J. Chem. Soc. Dalton Trans. (1991) 285–292.
[34] H.J. Zhang, P. Boutinaud, A. Garcia, J.P. Chaminade, C. Fouassier, Solid State Commun. 85 (12) (1993) 1031–1034.